IEEE Access
Multidisciplinary ⋮ Rapid Review ⋮ Open Access Journal

Received July 29, 2019, accepted September 19, 2019, date of publication September 24, 2019, date of current version October 10, 2019.

Digital Object Identifier 10.1109/ACCESS.2019.2943513

Research on Eigenvalue Analysis Method in Multi-Surface Metal Shell Vibratory Gyro

NING LIU[1] AND ZHONG SU[1,2]

[1]Beijing Key Laboratory of High Dynamic Navigation Technology, Beijing Information Science and Technological University, Beijing 100101, China
[2]School of Automation, Beijing Institute of Technology, Beijing 100081, China

Corresponding author: Ning Liu (ning.liu@bistu.edu.cn)

This work was supported in part by the National Natural Science Foundation of China under Grant 61801032, in part by the Beijing Natural Science Foundation under Grant 3184046, in part by the General Project of Science and Technology Program of Beijing Education Commission under Grant 77F1910963, and in part by the Beijing Key Laboratory of High Dynamic Navigation Technology, Qin Xin Talents Cultivation Program, Beijing Information Science and Technology University, and Laboratory of Modern Measurement and Control Technology (Beijing Information Science and Technology University Ministry of Education).

ABSTRACT The metal shell vibratory gyro is a branch of Coriolis vibratory gyro, which has the advantage of overload resistance, simplify structure, low cost, wide range and long life. This paper focuses on multi-surface metal resonator. It is important that the eigenvalue analysis of multi-surface of hemisphere, cylinder and hyperbolic. Through analysis multi-surface characteristic, it presents a novel orthogonal curvilinear coordinate used machine error factor based on the traditional coordinate, which realizes boundary linear. We analyze its natural vibration characteristics, research on basic model distribution and built mode shape function of resonator; deeply research on dynamics characteristics of resonator under the condition of angular rate input, establish dynamics equation of multi-surface fusion metal shell vibratory gyroscope based on thin shell mechanics theory of elastic mechanics, solve out the eigenvalue of the resonator, and we also analyze this eigenvalue characteristics to lay the foundation of the follow-up study of the theory of the metal shell vibratory gyroscope. We test the gyro's temperature performance on the last. Finally, we test on the metal shell vibratory gyroscope, the ranges to ±3600°/s, zero-bias stability is 7.862°/h (25 °C), angular random walk is 1.487°/h$^{1/2}$.

INDEX TERMS Vibratory gyro, eigenvalue analysis, multi-surface metal shell, metal shell vibratory gyroscope.

I. INTRODUCTION

The ability of range and overload resistance of the traditional metal shell vibratory gyroscope like cylinder-shaped, cone-shaped, rotating parabolic-shaped, is restricted by its own structure. So that the traditional metal shell vibratory gyroscope cannot be used to measure angular rate under the condition of high overload, wide-range [1], [2]. The typical axisymmetric shells include cylinder shell, hemisphere shell, paraboloidal shell and conical shell. For axisymmetric shell gyros, cylinder shell and hemisphere shell are the most widely used. Watson Industries Inc., Innalabs Holding Inc. and BAE have kinds of cylinder vibratory gyros which are wildly used in low and medium accuracy angular rate measurements fields, including vehicle navigation, oil exploration etc. They use the piezoelectric element which is attached on the cylinder wall to detect input angular rate [3]–[8]. Innalab Holding develops two-level cylinder to improve the quality of stand wave, sticks piezoelectric element to the bottom of cylinder to improve the drive efficiency and sensitivity [9]–[11]. Loveday, Kristiansen, Shangchun Fan, et al. have deeply studied on the vibration characteristics, dynamic equation, error analysis of the cylinder vibratory gyros, and formed a whole theory [12], [13].

Reasonable selection coordinate system to describe the resonator's dynamic characteristics is of crucial importance for this kind of axisymmetric shell vibratory gyroscope. In literature [14] and [15], the author studies cylindrical structures by selecting cylindrical coordinate. In literature [16], semi-spherical surface structure resonator is studied by selecting the spherical coordinate. In the literature [17]–[19], the conical structure is studied by selecting a conical coordinate. Leissa et al., described the vibration characteristics of composite structure by using the orthogonal

The associate editor coordinating the review of this manuscript and approving it for publication was Zhenbao Liu.

curvilinear coordinates, such as cylinder, cone, frustum, paraboloid shaped structure, and give a systematic exposition of the characteristics of this kind of coordinates and related mechanical properties [20], [21]. The resonator is of multi-curved surface fusion structure, which involves a variety of structural features, and cannot be accurately described in typical coordinates such as spherical and cylindrical ones [21]. Leissa et al., used the orthogonal curvilinear coordinate to describe the vibration characteristics of the complex shell, which is of great significance to the study of such structures.

For axisymmetric shell vibratory gyroscope, modal analysis is important too, but often in the process of theoretical analysis of gyro ignored. One of the important reasons is that calculation and analysis of vibration is very complex, and it is difficult to find the analytical solution in most cases [22]. The famous scholar Leissa et al., using Rayleigh-Ritz method, through the numerical simulation calculation, gives a set of three-dimensional vibration shell of vibration mode analysis method. Scholar Tzou et al. in the study of the active vibration mode control of three-dimensional shell, present the vibration modal analytical method based on analytical method for conical shells, rotating paraboloid shells and cylindrical shells [23]. The research of dynamic problems of Resonators mainly focus on mechanical properties of the Resonator under the action of Coriolis force. For the dynamic problem of this kind of axisymmetric shell resonator gyro, two methods are adopted at present: energy principle of elasticity mechanics [24], [12]; the solution of the balance differential equation [25].

Through analysis of the above three problems, this paper aims to put forward a kind of eigenvalue analysis method for the metal shell vibratory gyroscope of multi-surface fusion structure form. The former solves out the dynamic equation and the equivalent dynamic equation by establishing the mechanical kinetic energy, mechanical potential energy, and external potential energy, and using the Lagrange method. Introducing the effect of Coriolis force, the latter obtains the dynamic equation under the action of Coriolis force by establishing the balance differential equation of vibration, and by using the method of thin shell theory analysis, and then uses Bubonov Galerkin method to solve the equivalent dynamic equation. Both similarity is that the natural frequency and precession factor of resonator is obtained by equivalent dynamics equation, and the premise of similarity is to get vibration type function of resonator. Both have advantages and disadvantages.

II. THE ANALYSIS OF LIMITATIONS OF ORTHOGONAL CURVILINEAR COORDINATE SYSTEM

The resonator has a structure of thin shell. To study and analyze this kind of thin shell problems, people usually adopt the theory of plates and shells, the basis of which is the assumption of Kirchhoff-Love. The orthogonal curvilinear coordinate system represents points in space using the angle between the normal of the surface of the shell and the rotation axis, direction of rotation angle and thickness direction.

For the established orthogonal curvilinear coordinate system, there are some limitations. The emphasis is put on main curvature radius $\rho_1 = \infty$ for a shell with a curvature of 0. There is no problem in the description of the specific mechanical process, but in the process of analytic calculation, it will directly affect the nature of the whole calculation. For the resonator of multi-curved surface fusion structure, the cylindrical structure of its middle part is a typical shell with a curvature of 0. The principal curvature radius of the cylindrical surface structure is $\rho_1 = \infty$ in the coordinate constraint relation.

In the literature [20], the author also encountered similar problems in the vibration analysis of conical shells, but there is no solution. In [29], the analysis of thin shell vibration mechanics problems also uses the coordinate system. Neither does it give a method to solve limitation problem of this kind of coordinate. In order to solve this problem, this paper presents the use of rotating parabolic structure instead of cylindrical surface structure, and confines the curve errors of both within the processing error, as shown in Fig.1.

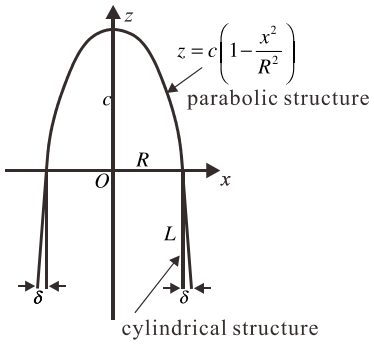

FIGURE 1. Equivalent curve diagram.

In the graph, the maximum deviation of the rotating parabolic surface and the cylindrical surface profile is represented by δ, and it should be less than the processing error of structure; c is the distance between parabolic vertex and coordinate origin. Therefore, the parabolic coordinate equation is

$$z = c\left(1 - \frac{x^2}{R^2}\right) \tag{1}$$

Using the coordinate relation, we can get

$$c = -\frac{LR^2}{\delta\,(\delta + 2R)} \tag{2}$$

In the actual machining process, the resonator is processed by the advanced numerical control center, the error is 0.005mm. So it is considered that there is an error in the machining process of the cylindrical part of the resonator,

$\delta = 0.005$mm. As a result, the radius of curvature of the equivalent cylindrical surface is obtained as follow:

$$\begin{aligned}\rho_1 &= -\frac{\delta\,(\delta+2R)}{L\cos^3\varphi}\\ \rho_2 &= -\frac{\delta\,(\delta+2R)}{L\cos\varphi}\end{aligned} \tag{3}$$

Synthesize the research status of metal shell resonator gyro at home and abroad, the resonator maximum height is 30mm, the maximum diameter is 43mm, then L = 30mm, R = 21.5mm. The equations, fully meet the requirements, so this method is feasible. After the numerical substitution, fully meet the requirements, so the method is feasible.

To sum up, we can obtain the constraint relationship of the three main structures of resonator after the equivalent processing.

$$\begin{aligned}&\texttt{Hemesphere}:\ \rho_1 = R,\quad \rho_2 = R\\ &\text{Cylinder}:\ \rho_1 = -\frac{\delta\,(\delta+2R)}{L\cos^3\varphi},\quad \rho_2 = -\frac{\delta\,(\delta+2R)}{L\cos\varphi}\\ &\texttt{Parabolic}:\ \rho_1 = \frac{-R^4S^2\sqrt{R_b^2-R^2}}{\left[\left(R_b^2-R^2\right)R^2\sin^2\varphi - R^2S^2\cos^2\varphi\right]^{\frac{3}{2}}},\\ &\qquad\rho_2 = \frac{R^2\sqrt{R_b^2-R^2}}{\left[\left(R_b^2-R^2\right)R^2\sin^2\varphi - R^2S^2\cos^2\varphi\right]^{\frac{1}{2}}}\end{aligned} \tag{4}$$

III. NATURAL VIBRATION OF THE RESONATOR

A. VIBRATION MODE RESEARCH OF THE RESONATOR

At any point on the resonator there is simple harmonic oscillation with a frequency, the displacement function of which can be expressed as [20]

$$\begin{cases} u_\varphi = \hat{U}e^{j\omega_n t}\\ u_\upsilon = \hat{V}e^{j\omega_n t}\\ u_\theta = \hat{W}e^{j\omega_n t}\end{cases} \tag{5}$$

Among them, $\hat{U}$, $\hat{V}$, $\hat{W}$ are Rayleigh functions of inherent vibration mode of certain inextensible thin shell, that is, vibration mode function. ω_n is natural angular frequency of vibration; t is for time. When studying the problem of vibration mode, it is assumed that the time cannot be correlated with the other variables, and the vibration periods of the points on the resonator are the same.

In the study of the vibration process of the resonator, the assumption that the middle plane of the shell cannot be stretched is used. That is, the equation for shell-bending is equal to zero by three components of tangential deformation [26], [27]. Then, we have

$$\varepsilon_{\varphi\varphi} = \varepsilon_{\theta\theta} = \varepsilon_{\varphi\theta} = 0 \tag{6}$$

Thus, can obtain:

$$\begin{cases} \dfrac{\partial u_\varphi}{\partial\varphi} + u_\upsilon = 0\\ \dfrac{\partial u_\theta}{\partial\theta} + u_\varphi\cos\varphi + u_\upsilon\sin\varphi = 0\\ \dfrac{1}{r_z}\left(\dfrac{\partial u_\varphi}{\partial\theta} - u_\theta\cos\varphi\right) + \dfrac{\frac{\partial u_\theta}{\partial\varphi}}{\rho_z} = 0\end{cases} \tag{7}$$

Since the Resonator has an axisymmetric distribution, the time can be separated, and the formula (7) can be simplified as:

$$\begin{cases} \dfrac{\partial\hat{U}}{\partial\varphi} + \hat{W} = 0\\ \dfrac{\partial\hat{V}}{\partial\theta} + \hat{U}\cos\varphi + \hat{W}\sin\varphi = 0\\ \dfrac{1}{r_z}\left(\dfrac{\partial\hat{U}}{\partial\theta} - \hat{V}\cos\varphi\right) + \dfrac{\frac{\partial\hat{V}}{\partial\varphi}}{\rho_z} = 0\end{cases} \tag{8}$$

By the method of separation of variables [28], the corresponding vibration mode function can be solved. First, assume vibration mode function along the thickness direction as

$$\hat{W} = f(\varphi)\cos(n\theta) \tag{9}$$

In equation, $f(\varphi)$ is a function of variable φ, n is vibration order of the resonator.

Substitute equation (9) into 1 of the equation (8), then

$$\hat{U} = -\int f(\varphi)\,d\varphi\cos(n\theta) \tag{10}$$

Substitute equation (9) into 2 of the equation (8), then for the same reason

$$\hat{V} = \frac{\sin(n\theta)}{n}\left[\cos\varphi\int f(\varphi)\,d\varphi - f(\varphi)\sin\varphi\right] \tag{11}$$

Substitute equation (10) and (11) into 3 of the equation (8), after simplification, we can get the (12)

$$\begin{aligned}&\frac{1}{r_z}\left[n\int f(\varphi)\,d\varphi - \frac{\cos\varphi}{n}\left(\cos\varphi\int f(\varphi)\,d\varphi - f(\varphi)\sin\varphi\right)\right]\\ &\quad - \frac{1}{\rho_z n}\left[\sin\varphi\int f(\varphi)\,d\varphi + f'(\varphi)\sin\varphi\right] = 0\end{aligned} \tag{12}$$

Observe equation(12), and assume $\int f(\varphi)d\varphi = F$, which is known as the characteristic function :

$$f(\varphi) = F';\quad f'(\varphi) = F'' \tag{13}$$

Substitute the assumption and equation (13) into equation (12), then get (14)

$$\begin{aligned}&\left(\rho_z n^2 - \rho_z\cos^2\varphi - r_z\sin\varphi\right)F + \sin\varphi\cos\varphi\rho_z F'\\ &\qquad - \sin\varphi r_z F'' = 0\end{aligned} \tag{14}$$

Observe equation(14), the solution of F is also equivalent to the solution of the vibration mode function in 3 directions.

For the resonator of whose curvature radius is of the piecewise function, its vibration mode function is expressed

in piecewise. Substitute r_z, ρ_z, using Maple to solve [29], we can get (15)

$$\begin{aligned} F &= C_1 \left[\cos(2\varphi) - 1\right]^{\frac{\rho_1-\rho_2}{4\nu+4\rho_2}} \\ &\left[\frac{1}{2}\cos(2\varphi) - \frac{1}{2}\right]^{\frac{2\nu+2\rho_2+\sqrt{4(\rho_2+\nu)(\rho_1+\nu)n^2+(\rho_1-\rho_2)^2}}{4\nu+4\rho_2}} \Im_1 \\ &+ C_2 \left[\cos(2\varphi) - 1\right]^{\frac{\rho_1-\rho_2}{4\nu+4\rho_2}} \sqrt{\cos(2\varphi)+1} \\ &\left(\frac{1}{2}\cos(2\varphi) - \frac{1}{2}\right)^{\frac{2\nu+2\rho_2+\sqrt{4(\rho_2+\nu)(\rho_1+\nu)n^2+(\rho_1-\rho_2)^2}}{4\nu+4\rho_2}} \Im_2 \end{aligned} \tag{15}$$

Among them, C_1, C_2 are arbitrary constants, and their concrete value depends on the initial value of the structural part of the vibration mode function. The concrete expressions of $\Im_1$, $\Im_2$ are as follows

$$\begin{aligned} \Im_1 &= \sum_{i=0}^{\infty} \frac{\left[\frac{1}{2}\cos(2\varphi) + \frac{1}{2}\right]^i \Gamma(n_1, i)\,\Gamma(n_2, i)}{i!\Gamma\left(\frac{1}{2}, i\right)\Gamma\left(\frac{1}{2}, i\right)}; \\ \Im_2 &= \sum_{i=0}^{\infty} \frac{\left[\frac{1}{2}\cos(2\varphi) + \frac{1}{2}\right]^i \Gamma(n_3, i)\,\Gamma(n_4, i)}{i!\Gamma\left(\frac{3}{2}, i\right)\Gamma\left(\frac{3}{2}, i\right)} \end{aligned} \tag{16}$$

In last equation, $\Gamma(\cdot)$ represents Gamma function when factorial calculation is carried out.

$$\begin{aligned} n_1 &= \frac{\sqrt{4(\rho_2+\nu)(\rho_1+\nu)n^2+(\rho_1-\rho_2)^2} - \rho_2 + \rho_1}{4\nu+4\rho_2} \\ n_2 &= \frac{\sqrt{4(\rho_2+\nu)(\rho_1+\nu)n^2+(\rho_1-\rho_2)^2} + 3\rho_2 + 2\nu - \rho_1}{4\nu+4\rho_2} \\ n_3 &= \frac{\sqrt{4(\rho_2+\nu)(\rho_1+\nu)n^2+(\rho_1-\rho_2)^2} + 5\rho_2 + 4\nu - \rho_1}{4\nu+4\rho_2} \\ n_1 &= \frac{\sqrt{4(\rho_2+\nu)(\rho_1+\nu)n^2+(\rho_1-\rho_2)^2} + \rho_2 + 2\nu + \rho_1}{4\nu+4\rho_2} \end{aligned}$$

When calculating the vibration mode, we can only consider the vibration of the middle plane curve of the resonator, so the thickness $\nu = 0$. Thus, the formula (15) can be simplified. Substituting (15) into the equation (9) - (11), we can solve out the vibration mode function of the resonator.

Then the vibration mode function of the resonator can be solved

$$\begin{aligned} \hat{U} &= -F\cos(n\theta) = U\cos(n\theta) \\ \hat{V} &= \frac{\left(F\cos\varphi - F'\sin\varphi\right)}{n}\sin(n\theta) = V\sin(n\theta) \\ \hat{W} &= F'\cos(n\theta) = W\cos(n\theta) \end{aligned} \tag{17}$$

By analyzing the working process of the resonator, the initial condition of the vibration mode function of the resonator can be determined. During the working process of the resonator, the displacement of the top restrained end of it is 0, and the vibration mode in this position should also be 0 [30] when it is in the position. Then

$$\begin{aligned} U|_{\varphi=\varphi_t} &= -F = 0 \\ V|_{\varphi=\varphi_t} &= \frac{\left(F\cos\varphi - F'\sin\varphi\right)}{n} = 0 \\ W|_{\varphi=\varphi_t} &= F' = 0 \end{aligned} \tag{18}$$

According to the formula, we can solve the initial value involved in the vibration mode function of the resonator. Firstly, the initial value of hemispherical shape is solved. Then when the coefficient is calculated, the cylindrical surface structure is solved out on the basis of hemispherical surface. Similarly, the solution of rotational hyperboloid structure can be done. When the theoretical derivation is carried out, the size of the support angle needed in the actual engineering of the resonator restraint end is ignored, setting $\varphi_t = 0$.

Combining with the 3 main structures of the resonator, make analysis of the eigenfunction of vibration mode of the resonator:

(1) Hemispherical surface structure

Substitute $\rho_1 = R$, $\rho_2 = R$ into equation (15), we can get

$$F = \sqrt{2}\sin\varphi\left(\frac{\sqrt{2}\cos\varphi - 2}{2\cos\varphi + 2}\right)^{\frac{n}{2}} \tag{19}$$

It can be seen that, at the bottom of the hemispherical structure, when $\varphi = \pi/2$, the corresponding vibration mode function can be obtained. At the same time, the vibration mode function of the hemispherical structure can be used as the initial value of the solution of cylindrical surface structure. This value can be used as the initial condition of cylindrical surface structure.

(2) Cylindrical surface structure

Substituting the constraint relation of the cylindrical surface structure into equation(15), we can get the eigenfunction of the resonator in the cylindrical structure.

$$F = \cos^n(\varphi)\left(1 - \cos(2\varphi)\right)^{\frac{1}{2}-\frac{n}{2}} \tag{20}$$

(3) Rotating hyperboloid structure

Substituting the constraint relation of the rotating hyperboloid structure into equation (15), we can get the eigenfunction of the resonator in the rotating hyperboloid structure.

$$\begin{aligned} F &= \left(\cos(2\varphi) - 1\right)^{\frac{1+n}{2}} \\ &\left(-4\sqrt{\left[R_b^2 - R^2 + S^2\right](1+\cos(2\varphi))}S\right. \\ &+ 2\cos(2\varphi)R_b^2 - 2\cos(2\varphi)R^2 \\ &\left.+ 4\cos(2\varphi)S^2 - 2R_b^2 + 2R^2 + 4S^2\right)^{-\frac{n}{2}} \end{aligned} \tag{21}$$

The eigenfunction of the corresponding structure is obtained, then, according to the equation(17), the vibration mode function of the corresponding structure can be obtained. In the process of numerical analysis, a set of initial parameters is given at first, as shown in Table 2. This parameter is

TABLE 1. Simulation parameter list of resonator vibration mode.

Parameters	Concrete values
Radius of hemispherical structure :R	10
Height of cylindrical surface structure:L	9
Height of rotating hyperboloid: S	2
Bottom Radius of rotating hyperboloid: R_b	12
The thickness of the resonator h	0.5

TABLE 2. Finite element simulation parameters of resonator.

Parameter names	Concrete values
Radius of hemispherical structure :R	9mm
Height of cylindrical surface structure:L	8mm
Height of rotating hyperboloid: S	2mm
Bottom opening radius: R_b	12mm
The thickness of the resonator: h	0.5mm
Material density: ρ	8170kg/m^3
Young's modulus of materials: E	196.76GPa
Poisson's ratio of material: γ	0.3

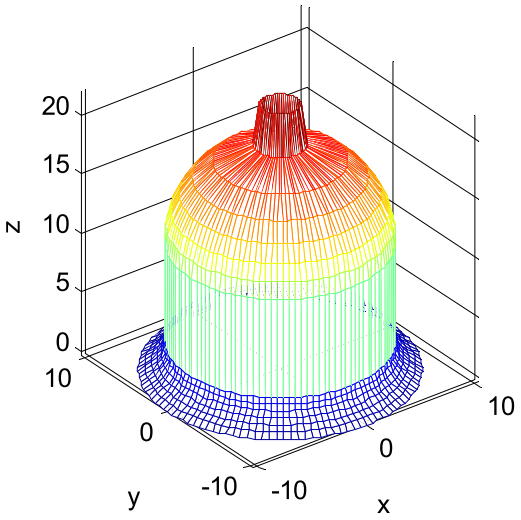

(a) Three-dimensional vibration mode

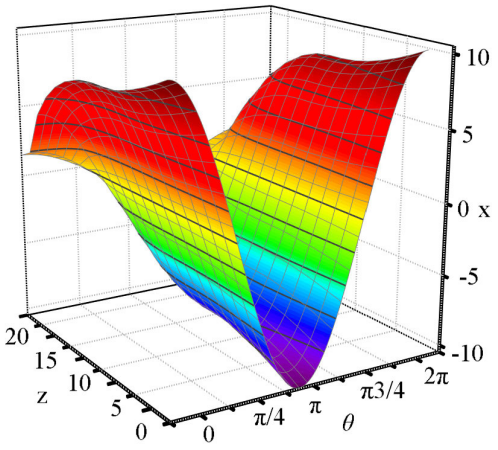

(b) Sectional view of vibration mode

FIGURE 2. 1 order vibration mode of resonator n = 1.

dimensionless and is only used to derive the vibration mode of the resonator.

In the analysis of vibration mode, low order vibration modes e of n = 1 to n = 4 are the main consideration. Numerical simulation analysis of vibration mode is made by Matlab. It is pointed out particularly that when the different vibration mode function is selected for each part of the structure, the range can be set manually. So the actual vibration mode of the resonator can be obtained as follow.

(1) Set $n = 1$, namely the 1 order vibration mode.

It can be seen from Fig.2 the main structure of resonator does not change and is in a swing mode when resonator works in 1 order vibration mode. The clock lip movement of resonator is as shown in Fig.3. And from its envelope wave of standing wave motion, it can be seen clearly that the resonator is in a swing mode.

(2) Set $n = 2$, that means, the resonator works in 1 order vibration mode.

As can be seen from Fig.4, when the resonator operates in the 2 mode, the bottom of the resonator is elliptical, and the overall structure has changed. The instantaneous curve of the clock lip and envelope curve of the standing wave are shown in Fig.5. By means of the polar coordinate envelope curve of the bell lip movement, vibration presents four antinodes and four nodes. So the vibration model is called 4 antinode vibration mode. The vibration mode can be selected as the working mode of the gyro, which contains one of the basic elements of the sensing Coriolis force: the radial motion of the particle. When the angular velocity is applied on the sensitive axis, the vibration mode can be deflected.

(3) Set $n = 3$, that means, the resonator works in 3 order vibration mode.

Fig.6 shows that at the bottom of clock lip presents three roses line shape which comprises 6 loops and 6 nodes (Fig.7), so that the vibration model is called 6 antinode vibration mode. The vibration mode can also be used to detect the

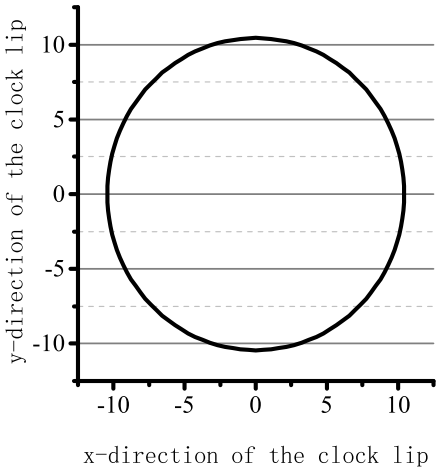

(a) Instantaneous motion curve of the clock lip

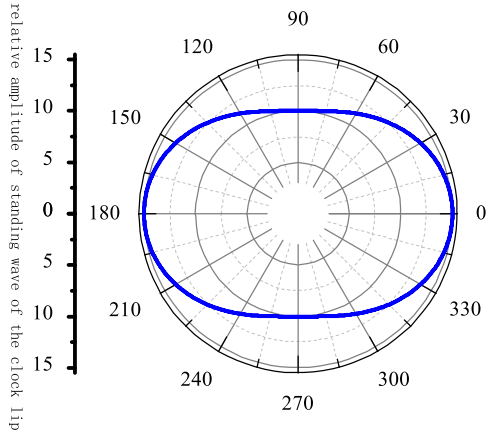

(b) Polar coordinate envelope curve

FIGURE 3. The clock lip motion of 1 order vibration mode resonator.

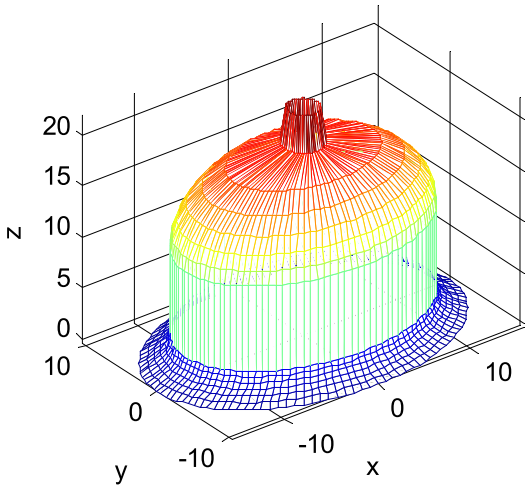

(a) Three-dimensional vibration mode

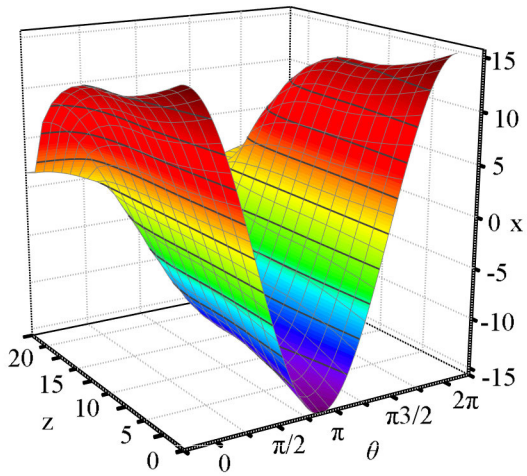

(b) Sectional view of vibration mode

FIGURE 4. 2 order vibration mode of resonator n = 2.

angular rate of the vibration mode, which also meet the basic conditions of Coriolis force detection, but will bring more complex calculations. Because of the influence of material characteristics and damping on the vibration mode analysis, the vibration modes that are analyzed all have ''zero crossing'' phenomenon. This is precisely the drawbacks of such analytical methods. In the next section, the finite element method is used to solve the problem for fully considering the material characteristics.

(4) Set n = 4, that means, the resonator works in 4 order vibration mode.

Similarly, it can be seen from the analysis of Fig.8, the vibration mode is of 8 antinode vibration mode which contains 8 loops and 8 nodes (Fig.9).

In summary, the numerical simulation analysis of vibrators with the first four order vibration mode function, derive the basic vibration mode of the resonator: swing vibration mode, 4 antinode vibration mode, 6 antinode vibration mode and 8 antinode vibration mode. In addition, analysis of the instantaneous motion and vibration mode envelope of clock lip provides a theoretical basis for vibration mode and standing wave precession of the subsequent Resonator.

B. ANALYSIS OF RESONATOR MODE

The finite element simulation software ANSYS is used to make mode analysis. The numerical solution of the actual vibration function of the resonator is obtained, and the basic vibration mode under actual working conditions and frequency distribution of the resonator are summarized. In the process of modeling and simulation, a set of general simulation parameters are selected, as shown in Table 2. The parameter is a dimensional value, unified under the standard unit.

ANSYS software is used to establish the three-dimensional finite element analysis model of the resonator. Diving by free mesh is shown in Fig.10 In the process of simulation, the unit type selected is Solid45.Restrictions are imposed at

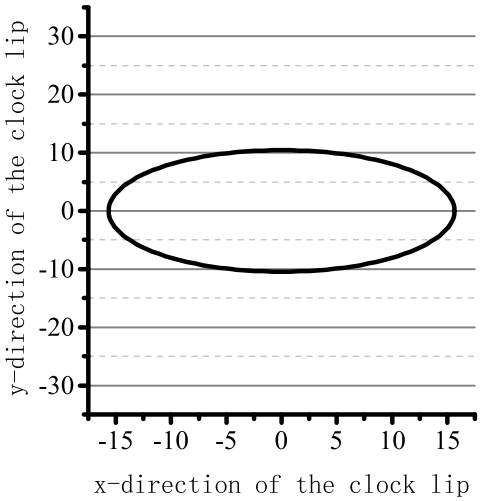

(a) Insta taneous motion curve

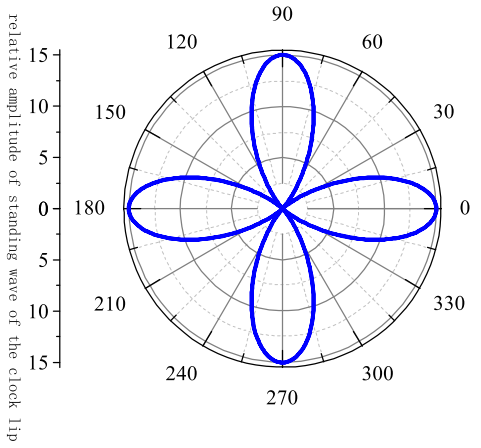

(b) Polar coordinate envelope curve

FIGURE 5. The clock lip motion of 1 order vibration mode resonator.

the constraint end of the resonator. Block Lanczo method is used to make modal analysis [3], [35]. The modal results of the first 8 order of the Resonator are shown in Figure 3.10

The first 8 order modal frequencies and the corresponding vibration mode can be analyzed from the finite element simulation results in Fig.11, as shown in Table 3.

The frequency distribution of first 8 order modal of the resonator ranges from 4447.2Hz ∼ 23283Hz, containing fundamental mode structure in Section 5. In addition to the 3 basic vibration mode analyzed in 3.1 quarter, there are also rotation vibration mode and the upper and lower vibration mode.

8 antinode vibration mode mentioned in analysis of vibration mode does not appear in the low frequency mode.

The results of modal analysis of the resonator shows that, by using the finite element simulation method, the vibration mode function of resonator obtained by the analytical method is verified. Both of them have the consistency. Low order vibration modes of the vibration mode function calculated by

TABLE 3. Analysis results of vibration mode.

Modal order	Frequency(Hz)	Vibration mode
1	4447.2	Swing mode (Fig.11(a)).
2	4480.8	Swing mode ((Fig.11(b))) differ with the swing vibration mode of 1 order mode by 90 °
3	7273.3	4 Antinode vibration mode (Fig.11(c))
4	7273.3	4 Antinode vibration mode (Fig.11(d)) , differ with 4 antinode vibration mode of 3 order mode by 45 °
5	14535	Rotating vibration mode (Fig.11(e))
6	19450	6 Antinode vibration mode (Fig.11(f))
7	19450	6 Antinode vibration mode (Fig.11(g)),differ with 6 antinode vibration mode of 5 order mode by 30 °
8	23283	Up and down vibration modes (Fig.11(a)).

analytical method, exists in results of finite element simulation. Although the 8 loop vibration mode does not appear, but in accordance with the laws of recursion, the 8 loop vibration mode should also occur in higher order modes. The 1 order modal vibration mode and the 2 modal vibration mode of the resonator are all of swing mode (n = 1), and the difference between them is about 90 degrees and the frequency difference is 33.5Hz. Both of them are almost at the same frequency point. The frequency difference between the two is caused by the non-uniform error introduced by the free mesh dividing, which can be ignored here. 3 order modal and 4 order modal vibration mode are 4 antinode vibration mode (n = 2), and difference of both is 45 degrees. The mode is the working mode of the resonator. The former is called excitation mode, the latter is called detection mode, and the two modes are coupled by Coriolis force. The 5 order modal vibration mode and the 8 order modal vibration mode are respectively the rotation mode and the upper and lower vibration mode. When the mode analysis is carried out, it is not calculated that there are two kinds of vibration modes, which also illustrates that the vibration mode function has some limitations and is not suitable for the two special modes, or in the case of considering the material parameters and structural damp, the resonator will increase the vibration mode. 6 order and 7 order modal vibration mode are 6 antinode vibration mode (n = 3), and difference of both is 30 degrees. The switching between the two modes can also be coupled by Coriolis force. In addition, with the increase of the vibration frequency, there will be more vibration modes, such as the 8 loop vibration mode, 10 loop vibration mode etc. But with the increase

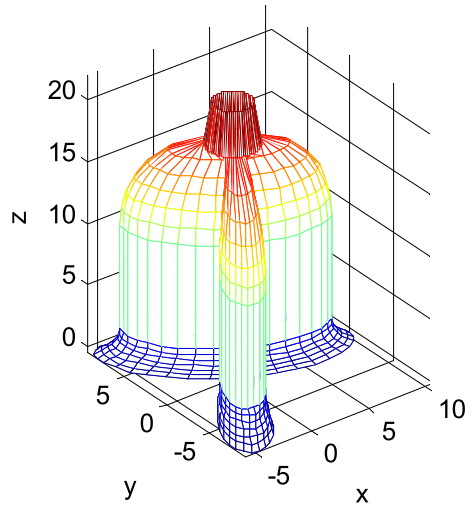

(a) Three-dimensional vibration mode

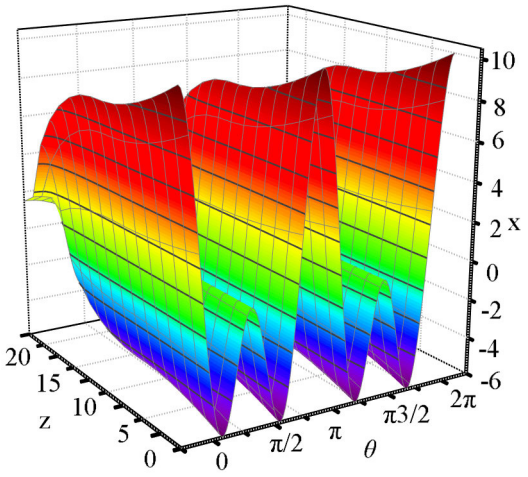

(b) Sectional view of vibration mode

FIGURE 6. 3 order vibration mode of resonator $n = 3$.

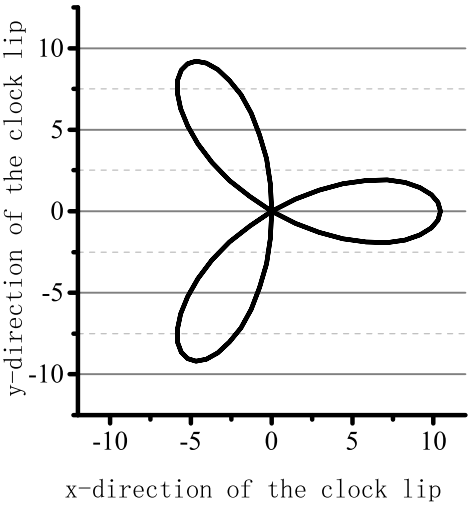

(a) Instantaneous motion curve of the clock lip of 3 order vibration mode

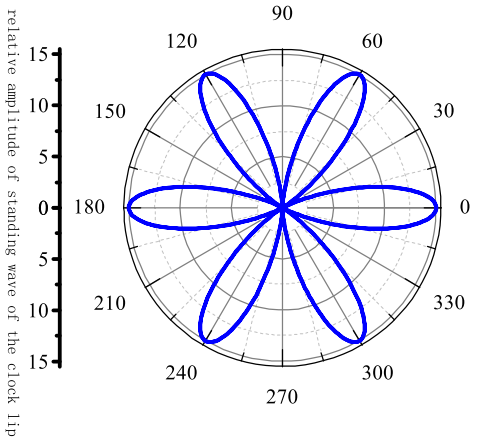

(b) Polar coordinate envelope curve of the clock lip motion of 3 order vibration mode

FIGURE 7. The clock lip motion shape of 3 order vibration mode of resonator.

of the number of loops, the vibration of the resonator will become more and more complicated. Therefore, the 4 loop vibration mode is adopted for the vibration mode selection. In the analysis process, only the low order modal distribution is analyzed so as to satisfy theoretical analysis of metal shell resonator gyro.

According to the vibration mode analysis and modal analysis results of the resonator, this paper lays special stress on analyzing 4 antinode vibration node. Through the ANSYS simulation software, the finite element simulation data is extracted, and the data of clock lip are analyzed.

The displacement curves of the excitation mode and detection mode of 10 vibrations on edge of the clock are draw respectively as shown in Fig. 12 and Fig.13.

Integrating Fig.10 and Fig.11, we can find that the clock lip under the condition of excitation mode and detection mode presents a typical 2 order vibration mode, and that the envelope curve of the particle motion trajectory at the bottom of the clock lip coincides well with that of the vibration mode function. There are differences in specific values mainly because of different simulation methods. Similarly, the vibration displacements in three directions (φ, ν, θ) are analyzed respectively. The overall trend is consistent with the trend of the three axis complex displacement, just different in values.

In excitation mode, it can be seen from Fig. 12 (b) that the motion of the particle at the edge of the clock lip edge satisfies the $\cos(2\theta)$ relation. And in detection mode, it can be seen from Fig.11 (b) that the motion of the particle at the edge of the clock lip edge satisfies the $\sin(2\theta)$ relation. The phase difference of 90 degrees between the two modes is shown in Fig.14.

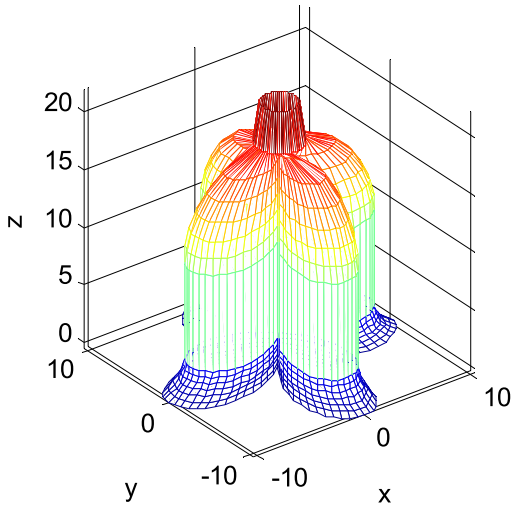

(a) Three-dimensional vibration mode

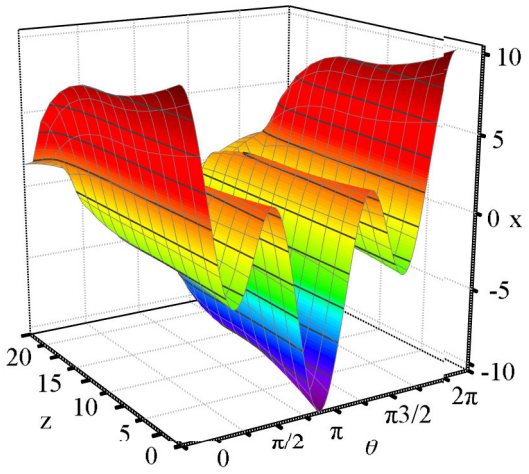

(b) Sectional view of vibration mode

FIGURE 8. 4 order vibration mode of resonator $n = 4$.

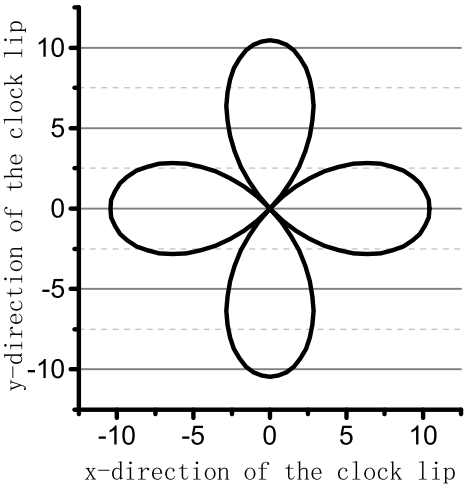

(a) Instantaneous motion curve of the clock lip of 4 order vibration mode

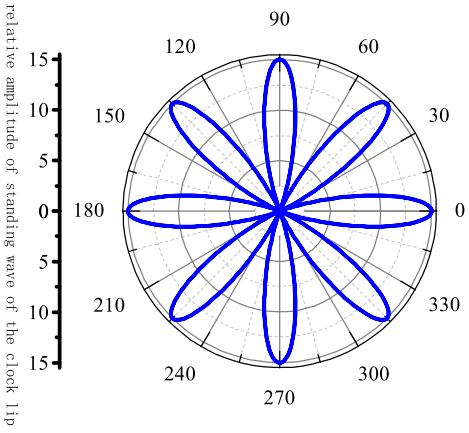

(b) Polar coordinate envelope curve of the clock lip motion of 4 order vibration mode

FIGURE 9. The clock lip motion shape of 4 order vibration mode of resonator.

Two orthogonal axes with phase difference of 90 degrees constitute Descartes coordinate system. So we set the excitation mode corresponding to the p axis (clock lip 0°), and set the detection mode corresponding to the q axis (clock lip 45°). The two inherent rigid axes form the orthogonal coordinate system of clock lip particles [31]. Similarly, in working mode, on each torus of the resonator exists the inherent rigid axes.

So, on the basis of the formula (5), the displacement of each point of the resonator is expand by natural mode of inextensible thin shell:

$$\begin{bmatrix} u_\varphi \\ u_\upsilon \\ u_\theta \end{bmatrix} = \begin{bmatrix} U\cos(n\theta) \\ V\sin(n\theta) \\ W\cos(n\theta) \end{bmatrix} p(t) + \begin{bmatrix} U\sin(n\theta) \\ -V\cos(n\theta) \\ W\sin(n\theta) \end{bmatrix} q(t) \tag{22}$$

Among them, $p(t)$, $q(t)$ is the time domain representation of the inherent rigid axes, mainly representing motion displacement on p axis and q axis and relating to time t. When the resonator is in the operating mode, n = 2.

C. DYNAMICS EQUATION OF RESONATOR

In the analysis of the dynamics problem of the resonator, this paper intuitively and effectively grasps the specific process of resonator by describing each particle movement of resonator and by using the equilibrium differential equation to solve dynamics equation.

1) THE ESTABLISHMENT OF DYNAMIC EQUATION

The motion of each point is considered as the motion of a particle. In orthogonal curvilinear coordinate system, each particle has displacement in three coordinate directions. For the particle $P(\varphi,\ \upsilon,\ \theta)$ on a resonator, the vector motion can be expressed as

$$\boldsymbol{\varphi} = u_\varphi\hat{\boldsymbol{\varphi}}, \quad \boldsymbol{\upsilon} = u_\upsilon\hat{\boldsymbol{\upsilon}}, \quad \boldsymbol{\theta} = u_\theta\hat{\boldsymbol{\theta}} \tag{23}$$

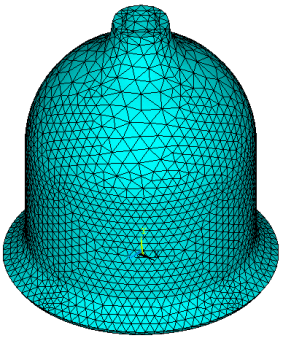

(a) Front view of the finite element model

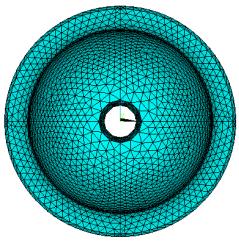

(b) Bottom view of the finite element model

FIGURE 10. The finite element model of resonator.

Among them, $\boldsymbol{\varphi}$ is displacement vector in the direction of φ, $\boldsymbol{\upsilon}$ is displacement vector in the direction of υ, and $\boldsymbol{\theta}$ is displacement vector in the direction of θ. $\hat{\boldsymbol{\varphi}}$, $\hat{\boldsymbol{\upsilon}}$, $\hat{\boldsymbol{\theta}}$ are unit vector in three directions. According to the above representation, the synthetic vector of the overall displacement of the particle P is expressed as

$$\mathfrak{R} = u_\varphi \hat{\boldsymbol{\varphi}} + u_\upsilon \hat{\boldsymbol{\upsilon}} + u_\theta \hat{\boldsymbol{\theta}} \tag{24}$$

When there is an external input angular rate $\boldsymbol{\Omega}$ on the sensitive axis, its expression in relation to inertial space is

$$\boldsymbol{\Omega} = \Omega\left(\cos\varphi\hat{\boldsymbol{\upsilon}} - \sin\varphi\hat{\boldsymbol{\varphi}}\right) = \Omega\cos\varphi\hat{\boldsymbol{\upsilon}} - \Omega\sin\varphi\hat{\boldsymbol{\varphi}} \tag{25}$$

According to the Coriolis theorem and Wallis formula, the absolute acceleration of the particle P relative to the inertial space is as follows

$$\boldsymbol{a} = \boldsymbol{a}_0 + 2\boldsymbol{\Omega}\times\mathfrak{R}' + \mathfrak{R}'' + \left[\boldsymbol{\Omega}'\times\mathfrak{R}\right] + \left[\boldsymbol{\Omega}\times\left[\boldsymbol{\Omega}\times\mathfrak{R}\right]\right] \tag{26}$$

Among them, $\boldsymbol{a}_0$ is the absolute acceleration of the particle P. $\mathfrak{R}''$ is the acceleration of the particle P; $\mathfrak{R}'$ is the velocity of the particle P. $\boldsymbol{\Omega}'$ is the angular acceleration of the particle P.

The formula (26) is expanded so that it can be obtained

$$\begin{aligned}
a_\varphi &= u_\varphi'' + \Omega' u_\theta\cos\varphi + 2\Omega u_\theta'\cos\varphi \\
&\quad - \Omega^2 u_\varphi\cos^2\varphi - \Omega^2 u_\upsilon\cos\varphi\sin\varphi \\
a_\upsilon &= u_\upsilon'' + \Omega' u_\theta\sin\varphi + 2\Omega u_\theta'\sin\varphi \\
&\quad - \Omega^2 u_\upsilon\sin^2\varphi - \Omega^2 u_\varphi\sin\varphi\cos\varphi \\
a_\theta &= u_\theta'' - \Omega^2 u_\theta - \Omega' u_\varphi\cos\varphi \\
&\quad - \Omega' u_\upsilon\sin\varphi - 2\Omega u_\varphi'\cos\varphi - 2\Omega u_\upsilon'\sin\varphi
\end{aligned} \tag{27}$$

Among them, a_φ is the acceleration in the direction of θ, a_υ is the acceleration in the direction of θ, is the acceleration in the direction of θ. According to Newton's second law of motion, it is known that the inertial force of the particle P influenced by the external angular velocity is

$$f_\varphi = -\rho a_\varphi, \quad f_\upsilon = -\rho a_\upsilon, \quad f_\theta = -\rho a_\theta \tag{28}$$

Substituting formula (28) into the balance differential equations, we can get the dynamic equation of the resonator rotating around symmetric axis at $\boldsymbol{\Omega}$ angular velocity under the action of external distributed load.

$$\begin{aligned}
&\frac{\partial\sigma_{\varphi\upsilon}}{\partial\upsilon} + \frac{1}{r_z}\left[\left(\sigma_{\varphi\varphi} - \sigma_{\theta\theta}\right)\cos\varphi + \frac{\partial\sigma_{\varphi\theta}}{\partial\theta} + \sigma_{\varphi\theta}\sin\varphi\right] \\
&\quad + \frac{1}{\rho_z}\left(\frac{\partial\sigma_{\varphi\varphi}}{\partial\varphi} + 2\sigma_{\varphi\upsilon}\right) - \frac{2\sigma_{\varphi\varphi}\frac{\partial\rho_1}{\partial\varphi}}{\rho_z^2} \\
&= \rho\begin{pmatrix} u_\varphi'' + 2\Omega u_\theta'\cos\varphi + \Omega' u_\theta\cos\varphi \\ -\Omega^2 u_\varphi\cos^2\varphi - \Omega^2 u_\upsilon\cos\varphi\sin\varphi \end{pmatrix} \\
&\frac{\partial\sigma_{\upsilon\upsilon}}{\partial\upsilon} + \frac{1}{r_z}\left[\left(\sigma_{\upsilon\upsilon} - \sigma_{\theta\theta}\right)\sin\varphi + \frac{\partial\sigma_{\upsilon\theta}}{\partial\theta} + \sigma_{\varphi\upsilon}\cos\varphi\right] \\
&\quad + \frac{1}{\rho_z}\left(\frac{\partial\sigma_{\varphi\upsilon}}{\partial\varphi} + \sigma_{\upsilon\upsilon} - \sigma_{\varphi\varphi}\right) - \frac{\sigma_{\varphi\upsilon}\frac{\partial\rho_1}{\partial\varphi}}{\rho_z^2} \\
&= \rho\begin{pmatrix} u_\upsilon'' + 2\Omega u_\theta'\sin\varphi + \Omega' u_\theta\sin\varphi \\ -\Omega^2 u_\upsilon\sin^2\varphi - \Omega^2 u_\varphi\sin\varphi\cos\varphi \end{pmatrix} \\
&\quad \frac{\partial\sigma_{\upsilon\theta}}{\partial\upsilon} + \frac{1}{r_z}\left(3\sigma_{\varphi\theta}\cos\varphi + 2\sigma_{\upsilon\theta}\sin\varphi + \frac{\partial\sigma_{\theta\theta}}{\partial\theta}\right) \\
&\quad + \frac{1}{\rho_z}\left(\sigma_{\upsilon\theta} + \frac{\partial\sigma_{\varphi\theta}}{\partial\theta} - \frac{\sigma_{\varphi\theta}}{r_z}\frac{\partial r_z}{\partial\varphi}\right) - \frac{\sigma_{\varphi\theta}\frac{\partial\rho_1}{\partial\varphi}}{\rho_z^2} \\
&= \rho\begin{pmatrix} u_\theta'' - 2\Omega u_\varphi'\cos\varphi - 2\Omega u_\upsilon'\sin\varphi \\ -\Omega^2 u_\theta - \Omega' u_\varphi\cos\varphi - \Omega' u_\upsilon\sin\varphi \end{pmatrix}
\end{aligned} \tag{29}$$

2) SOLUTIONS OF DYNAMIC EQUATIONS

Bubonov Galerkin method is usually used for solving the differential equation of dynamic equation (29). And it is a simple and effective method for the approximate solution of differential equations. This method, not only can solve the static problems but also can solve dynamic problems.

For the equation(29), the dynamic equation mainly based on stress and displacement is transformed into the dynamic equation based on displacement. Its basic form is

$$\begin{cases} D_1\left(u_\varphi, u_\varphi', u_\varphi'', u_\upsilon, u_\upsilon', u_\upsilon'', u_\theta, u_\theta', u_\theta''\right) = 0 \\ D_2\left(u_\varphi, u_\varphi', u_\varphi'', u_\upsilon, u_\upsilon', u_\upsilon'', u_\theta, u_\theta', u_\theta''\right) = 0 \\ D_3\left(u_\varphi, u_\varphi', u_\varphi'', u_\upsilon, u_\upsilon', u_\upsilon'', u_\theta, u_\theta', u_\theta''\right) = 0 \end{cases} \tag{30}$$

And, $D_1(\cdot)$, $D_2(\cdot)$, $D_3(\cdot)$ is the simplified form of the corresponding equation.

Because the equation is too complicated in the process of substitution, we pass over the introduction of simplification. This part of the calculation process can be calculated by Maple software [29]. Then the error function is obtained when calculating by Bubonov Galerkin method.

$$\tilde{\boldsymbol{L}} = D_1(\cdot)\hat{\boldsymbol{\varphi}} + D_2(\cdot)\hat{\boldsymbol{\upsilon}} + D_3(\cdot)\hat{\boldsymbol{\theta}} \tag{31}$$

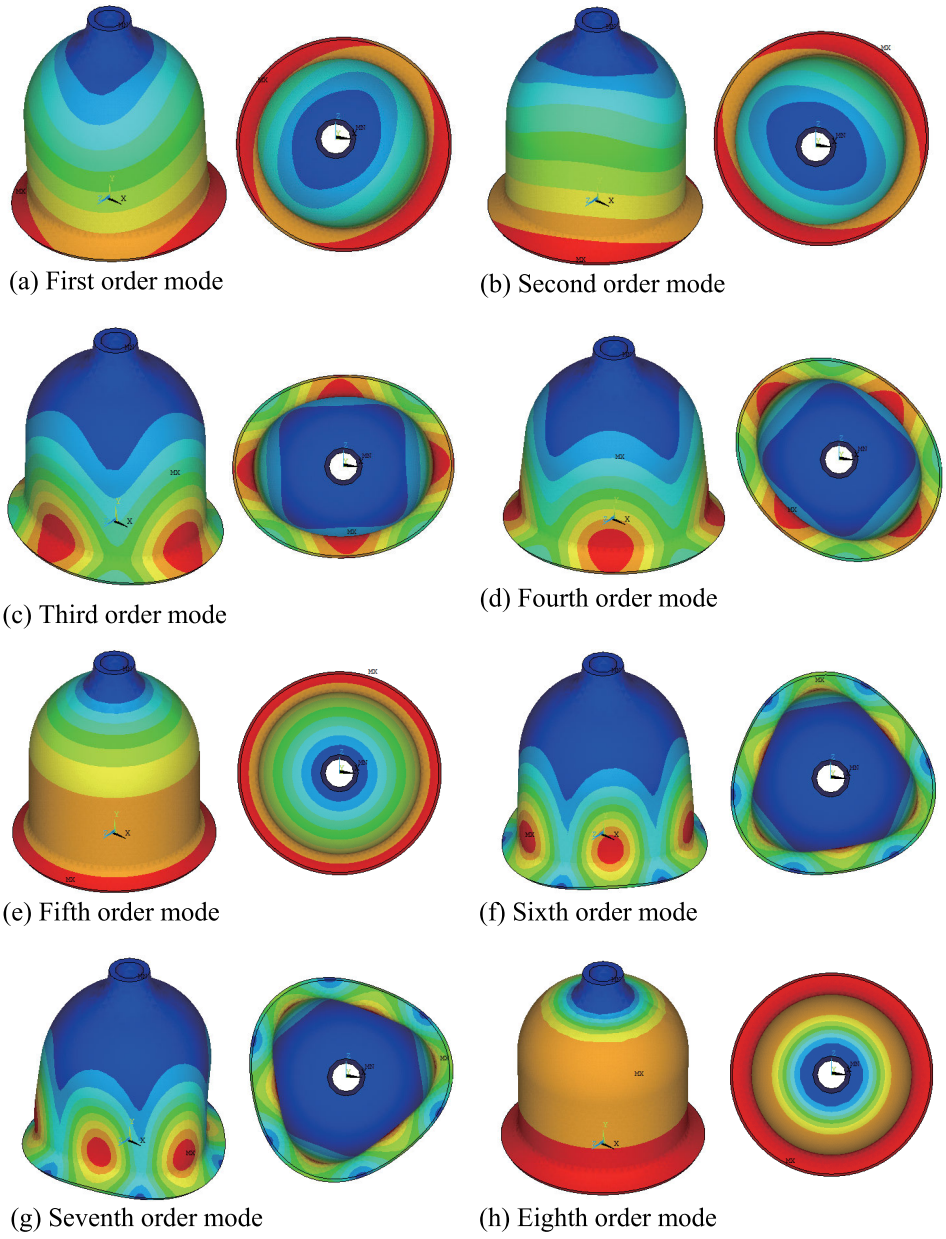

FIGURE 11. Analysis results of resonator mode.

The formula (22) is a general analytic form of the equation (30) in the case of n = 2. And combined with the formula (24), the vector displacement of the clock lip particle under the two order inherent rigid axes is obtained as follows

$$\begin{aligned}\mathfrak{R} &= u_\varphi\hat{\boldsymbol{\varphi}} + u_\upsilon\hat{\boldsymbol{\upsilon}} + u_\theta\hat{\boldsymbol{\theta}} \\ &= [U\cos(2\theta)p(t) + U\sin(2\theta)q(t)]\,\hat{\boldsymbol{\varphi}} \\ &\quad + [V\sin(2\theta)p(t) - V\cos(2\theta)q(t)]\,\hat{\boldsymbol{\upsilon}} \\ &\quad + [W\cos(2\theta)p(t) + W\sin(2\theta)q(t)]\,\hat{\boldsymbol{\theta}} \\ &= \left[U\cos(2\theta)\hat{\boldsymbol{\varphi}} + V\sin(2\theta)\hat{\boldsymbol{\upsilon}} + W\cos(2\theta)\hat{\boldsymbol{\theta}}\right]p(t) \\ &\quad + \left[U\sin(2\theta)\hat{\boldsymbol{\varphi}} - V\cos(2\theta)\hat{\boldsymbol{\upsilon}} + W\sin(2\theta)\hat{\boldsymbol{\theta}}\right]q(t)\end{aligned} \tag{32}$$

Use the above equation constructing orthogonal function, then

$$\begin{aligned}\tilde{\boldsymbol{\varphi}}_1 &= U\cos(2\theta)\hat{\boldsymbol{\varphi}} + V\sin(2\theta)\hat{\boldsymbol{\upsilon}} + W\cos(2\theta)\hat{\boldsymbol{\theta}} \\ \tilde{\boldsymbol{\varphi}}_2 &= U\sin(2\theta)\hat{\boldsymbol{\varphi}} - V\cos(2\theta)\hat{\boldsymbol{\upsilon}} + W\sin(2\theta)\hat{\boldsymbol{\theta}}\end{aligned} \tag{33}$$

Since $\tilde{\boldsymbol{L}}$ is orthogonal to the vectors $\tilde{\boldsymbol{\varphi}}_1$ and $\tilde{\boldsymbol{\varphi}}_2$ respectively, the differential equations are obtained

$$\begin{cases} \iiint\limits_V \begin{bmatrix} D_1(\cdot)\,U\cos(2\theta) \\ +D_2(\cdot)\,V\sin(2\theta) \\ +D_3(\cdot)\,W\cos(2\theta) \end{bmatrix} d\varphi dv d\theta = 0 \\ \iiint\limits_V \begin{bmatrix} D_1(\cdot)\,U\sin(2\theta) \\ -D_2(\cdot)\,V\cos(2\theta) \\ +D_3(\cdot)\,W\sin(2\theta) \end{bmatrix} d\varphi dv d\theta = 0 \end{cases} \tag{34}$$

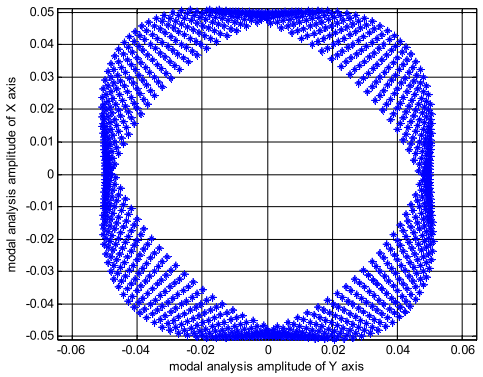

(a) Motion trajectory plan of clock lip particle

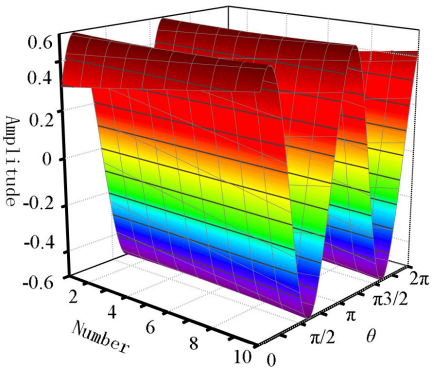

(b) Motion stereogram plan of clock lip particle

FIGURE 12. Clock lip edge vibration of excitation mode.

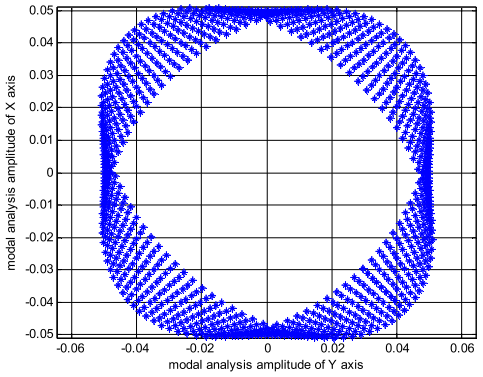

(a) Motion trajectory plan of clock lip particle

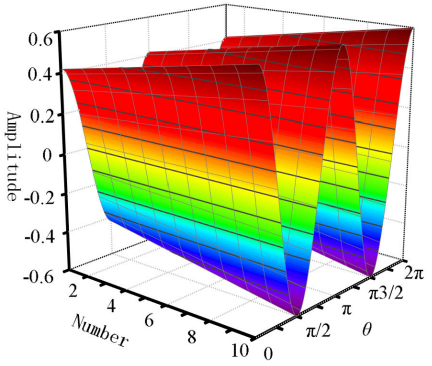

(b) Motion stereogram plan of clock lip particle

FIGURE 13. Clock lip edge vibration of detection mode.

Simplifying the results, we can obtain the equivalent dynamic equation describing the two order natural vibration mode of the ideal resonator

$$\begin{cases} m_0 p''(t) - 2\Omega b_0 q'(t) + c_0 p(t) + c_1 q(t) = 0 \\ m_0 q''(t) + 2\Omega b_0 p'(t) + c_0 q(t) + c_1 p(t) = 0 \end{cases} \tag{35}$$

In this equation, the alpha symbols are shown in Appendix.

By formula (35) we can solve the precession factor corresponding to the resonator and inherent frequency of resonator characteristics, meanwhile verify this kind of metal shell vibratory gyroscope with typical characteristics, of which the resonator edge can be equivalent to a two-dimensional spring mass movement. For the solution of formula (35), the numerical simulation method can be used.

Precession factor for resonator is [25]

$$\begin{aligned} K &= \frac{b_0}{2m_0} \\ &= \frac{2\rho\pi \int_{-\frac{h}{2}}^{\frac{h}{2}} \int_{\varphi_t}^{\varphi_b} VW \sin\varphi d\varphi dv}{-2\rho\pi \int_{-\frac{h}{2}}^{\frac{h}{2}} \int_{\varphi_t}^{\varphi_b} \left(U^2 + V^2 + W^2\right) d\varphi dv} \\ &= -\frac{\int_{\varphi_t}^{\varphi_b} VW \sin\varphi d\varphi}{\int_{\varphi_t}^{\varphi_b} \left(U^2 + V^2 + W^2\right) d\varphi} \end{aligned} \tag{36}$$

Formula (36) shows that the precession factor of resonator has nothing to do with material parameters of the resonator,

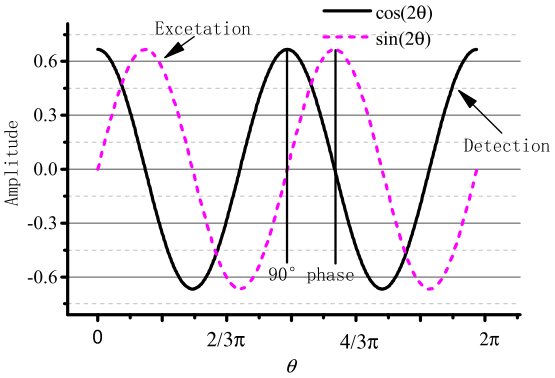

FIGURE 14. Relation of working modal.

but only has a relation with the vibration structure of the resonator. The natural frequency of the resonator is

$$\begin{aligned} \omega_n &= \sqrt{\frac{c_0}{m_0}} \\ &= \sqrt{\frac{\pi \int_{-\frac{h}{2}}^{\frac{h}{2}} \int_{\varphi_t}^{\varphi_b} (\eta_1 U + \eta_2 V + \eta_3 W + \eta_4) d\varphi dv}{-\rho\pi \int_{-\frac{h}{2}}^{\frac{h}{2}} \int_{\varphi_t}^{\varphi_b} \left(U^2 + V^2 + W^2\right) d\varphi dv}} \end{aligned}$$

$$= \sqrt{\frac{\int_{-\frac{h}{2}}^{\frac{h}{2}} \int_{\varphi_t}^{\varphi_b} (\eta_1 U + \eta_2 V + \eta_3 W + \eta_4)\, d\varphi dv}{-\rho \int_{-\frac{h}{2}}^{\frac{h}{2}} \int_{\varphi_t}^{\varphi_b} \left(U^2 + V^2 + W^2\right) d\varphi dv}}$$

$$= \sqrt{\frac{\int_{-\frac{h}{2}}^{\frac{h}{2}} \int_{\varphi_t}^{\varphi_b} (\eta_1 U + \eta_2 V + \eta_3 W)\, d\varphi dv + \int_{-\frac{h}{2}}^{\frac{h}{2}} \int_{\varphi_t}^{\varphi_b} \eta_4 d\varphi dv}{-\rho \int_{-\frac{h}{2}}^{\frac{h}{2}} \int_{\varphi_t}^{\varphi_b} \left(U^2 + V^2 + W^2\right) d\varphi dv}}$$

$$= \sqrt{\chi_1 + \chi_2} \tag{37}$$

Of which,

$$\chi_1 = \frac{\int_{-\frac{h}{2}}^{\frac{h}{2}} \int_{\varphi_t}^{\varphi_b} (\eta_1 U + \eta_2 V + \eta_3 W)\, d\varphi dv}{-\rho \int_{-\frac{h}{2}}^{\frac{h}{2}} \int_{\varphi_t}^{\varphi_b} \left(U^2 + V^2 + W^2\right) d\varphi dv},$$

$$\chi_2 = \frac{\int_{-\frac{h}{2}}^{\frac{h}{2}} \int_{\varphi_t}^{\varphi_b} \eta_4 d\varphi dv}{-\rho \int_{-\frac{h}{2}}^{\frac{h}{2}} \int_{\varphi_t}^{\varphi_b} \left(U^2 + V^2 + W^2\right) d\varphi dv}.$$

Natural frequency for the resonator is

$$f_n = \frac{\omega_n}{2\pi} \tag{38}$$

According to the formula(37), the influence of the natural frequency of the resonator is mainly composed of the following two parts: the material and the structure characteristics of the resonator itself, and the influence of the angular velocity. In the study of axisymmetric shell resonator gyro. Since the vibration frequency of the resonator is much larger than the angular velocity of the detection, both the square term of the angular rate and the derivative term are ignored. In this paper, the metal shell resonator gyro is mainly for a large measurement range, in field of which the input angular rate compared with the natural frequency is not a small variable. For this reason, it cannot be ignored.

For consideration of the numerical simulation requirements of equation (37), it is necessary to integrate the three main structural parameters of the resonator, and then substitute the coordinate constraint relations of each part to calculate effectively.

However, for a resonator with a hemispherical, cylindrical, or hyperboloid structure described by an orthogonal curvilinear coordinate system, there is no obvious structural distinction in the direction of $\hat{\boldsymbol{\varphi}}$. In hemispherical surface structure, its φ value is

$$\varphi \in \left[0, \frac{\pi}{2}\right]$$

As for the cylindrical surface structure, its φ value is in the vicinity of $\pi/2$. The same is true for the rotating hyperboloid structure, and its φ value is

$$\varphi \in \left(0, \frac{\pi}{2}\right]$$

All three have intersection, and cannot be used as signs of segmentation. The analysis of the vibration process of axisymmetric shell vibratory gyroscope shows that, the stiffness distribution of the free end is the most influential factor to its characteristic, and that the rest of the structure only provides the effective support and standing wave transmission for free end. Therefore, in the numerical simulation analysis, the structural parameters of the formula (35) are selected to calculate by the structural parameters of the rotating hyperboloid structure. However, in order to solve the vibration mode function of this part, it is need to use the structural parameters and constraint relationship between the hemispherical structure and the cylindrical structure. Therefore, it seems intuitively that it is the only use of the rotational hyperboloid structure. But in fact it is a combination of the structural characteristics of the three parts.

IV. RESONATOR CHARACTERISTIC TEST

A. NATURAL FREQUENCY TEST

The frequency domain characteristics of the resonator are tested by using the Solartron 1255B sweep frequency meter. The Resonator is processed by the method of Resonator mechanical balance, which makes the frequency split of the final Resonator at 0.3Hz. First, the frequency detection of dipole mode. The signal output frequency sweep meter is connected to the piezoelectric electrodes 1 and 5. The channel 1 is connected to the piezoelectric electrode 3. Channel 2 is connected to the piezoelectric electrode 7. The test results are shown in Fig.15 [1]. At this time, the excitation mode frequency of the Resonator is 6930.6Hz. Similarly, the output signal will sweep device is connected to the piezoelectric electrodes 2 and 6. The channel 1 is connected to the piezoelectric electrode 4. Channel 2 is connected to the piezoelectric electrode 8. The test results are shown in Fig.16, and the testing modal frequency of the Resonator is 6930.3Hz.

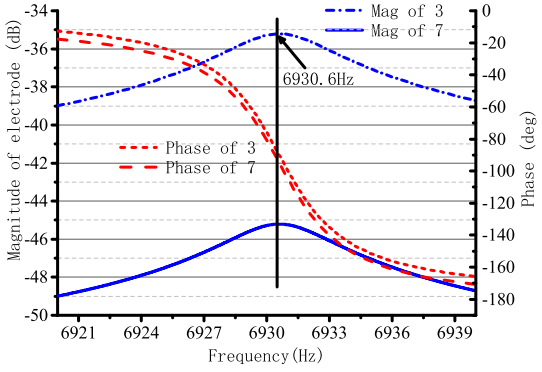

FIGURE 15. Sweep results for the excitation mode.

The results of the two groups were observed, and the output of the electrodes with the same function was different. In actual processing, material distribution and structure characteristics of resonator machining error of external factors lead to the structure is not completely symmetrical. It affects the distribution of the rigid axis of the resonator, which makes

the vibration mode shift, and causes the frequency deviation (This deviation is called frequency cracking) of the excitation mode and the detection mode, and this property is one of the inherent properties of metal shell vibratory gyroscopes.

For this problem, there are a large number of scholars to study, including the cup-type Resonator, hemispherical Resonator, ring Resonator, etc. There are two main methods: mechanical modification and circuit compensation [37], [38]. As for the metal shell vibratory gyro, its resonator structure is multi-surface fusion structure, which different from the general axisymmetric shell structure–there are significant differences in the mechanical balance adjustment mode. The main lip of the resonator is responsible for the regulation of the rigid shaft. At the same time, the piezoelectric electrode of the resonator is pasted on the bell wall, and close to the bell lip. So the subtle quality change will affect the whole rigid shafting distribution; the cutting is done on the lathe, it will cause damage to itself. Therefore, the mechanical balance of the resonator is adjusted by adopting a non-contact balance adjustment method, and the precise mechanical balance adjustment is realized by a pulse laser and a multi axis displacement platform [35], [36]. For the slight deviation of mechanical balance adjustment, we must rely on the circuit control technology to compensate.

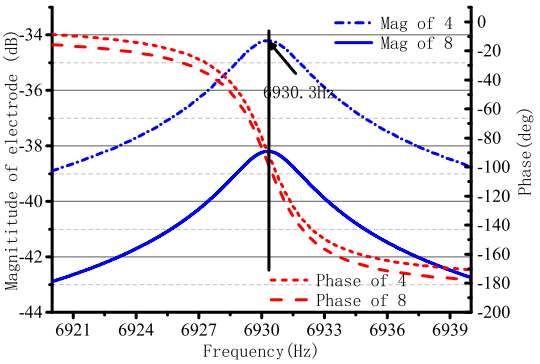

FIGURE 16. Sweep results for detection mode.

Figure 15 and Figure 16 shows that the natural frequency of the Resonator is 6930.6Hz. Using the same method, the remaining 10 sets of Resonators were tested, and the natural frequency range from 6720.1Hz to 7205.3Hz, a difference of 485.2Hz. The calculated Resonator natural frequency in the same range, which also confirms the derivation of mathematical models and the correctness of finite element simulation.

B. VIBRATION TESTING

Vibration mode test of resonator was tested by a vibrometer. Focus the laser vibrometer on the lip and adjust the signal generator. After the circuit system conditioning, resonator is excited vibration. The resonator was fixed on a precision rotating table and tested at 5° intervals. The test photographs are shown in Fig. 17. The test results are shown

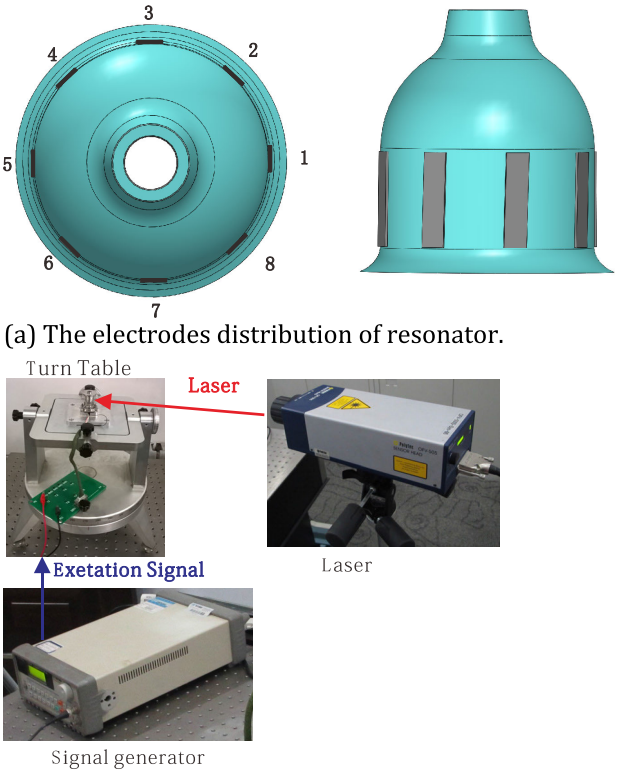

FIGURE 17. Mode shape test.

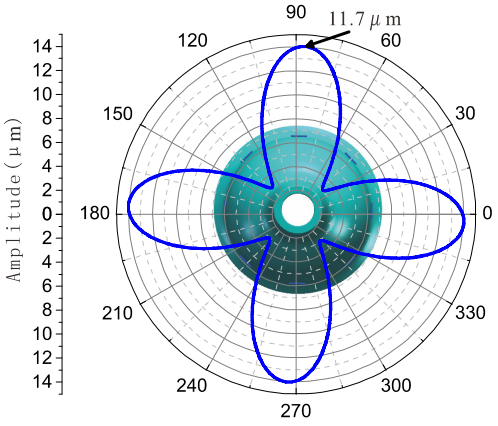

FIGURE 18. The result of test.

in Fig.18. Using the Polytec PSV-400 scanning vibrometer tests the radial displacement amplitude. The circumference of the resonator was divided in 72 parts. The active frequency is6930.3Hz, the amplitude is 5V. Using Matlab polar function plots the curve. When we test the resonator firstly, we didn't divide the circumference carefully. The node didn't find from the curve. The value of the amplitude helps us find the node (amplitude = 0).

It can be seen from Fig.18 that the bottom edge of the resonator exhibits a typical four-wave abdominal vibration

with a maximum amplitude of 11.7μm and the motion of the modified Resonator node is obvious. The ideal four-wave abdominal vibration mode is the same as that calculated in Section 2. But the test results show that the lobe is not completely symmetrical, which may include the Resonator processing error, the piezoelectric film paste process and other factors lead to.

V. PROTOTYPE TEST

According to the simulation results and hardware architecture design, the control circuit is designed and the metal shell vibratory gyro prototype is fabricated as shown in Fig.19. The gyro's control circuit is shown in Fig.19 (a) and prototype in Fig.19 (b).

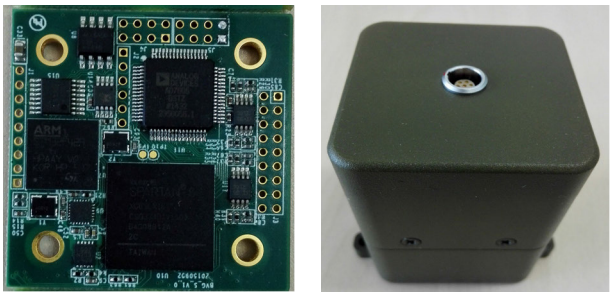

(a) Control circuit (b) Gyro prototype

FIGURE 19. Metal shell vibratory gyro prototype.

We will make the prototype for the turntable tracking test, as shown in Fig.20. The experiment temperature is 25°. The gyro's output is used RS-422 and the refresh time is 2ms.

FIGURE 20. Turntable test photo.

A. DYNAMIC TESTING

The metal shell vibratory gyro was started for 5 minutes, the control turntable was rotated by ± 600 °/s, ± 1200 °/s, ± 1800 °/s, ± 2400 °/s, ± 3000 °/s, ± 3600 °/s, and each angular rate of rotation is greater than 1.5 minute. The test results are shown in Fig.21, and it can be seen that the design of a large range of angular rate detection method to accurately track turntable run.

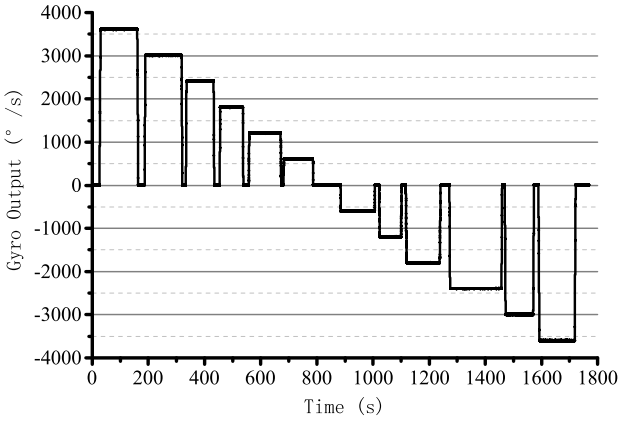

FIGURE 21. Turntable tracking test.

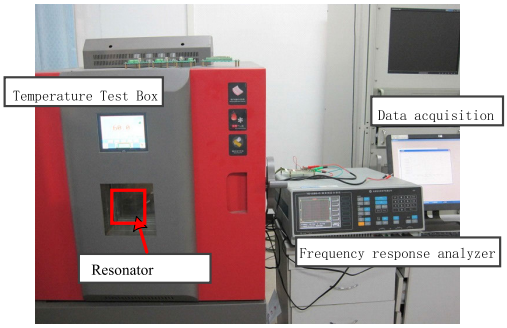

FIGURE 22. Temperature test.

To sum up, the range of gyro is 3600°/s, the scale factor linear is 1.2%.

B. TEMPERATURE TESTING

The temperature characteristics of the gyroscope are tested by using high and low temperature experimental equipment (the test photos are as follows).

Temperature mainly affects the material properties of the resonator, which is directly reflected in the natural frequency of the resonator. The test result is as shown.

The resonant frequency has a linear relationship with temperature, and the resonant frequency of the resonator increases with the increase of temperature. The gyroscope bias drifts under the influence of temperature, and its change trend is very obvious. The variation range of the gyroscope in the whole temperature range is large, so it cannot meet the actual application requirements, so temperature compensation must be carried out.

C. STATIC TESTING

The control turntable was stationary and the output signal of the metal shell vibratory gyro was recorded at an update rate of 200 Hz for 1 hour, as shown in Fig.24. Using the method in [42], the Allan variance of the metal shell vibratory gyro is shown in Fig.25.

$$m_0 = -\rho\pi \int_{-\frac{h}{2}}^{\frac{h}{2}} \int_{\varphi_t}^{\varphi_b} \left(U^2 + V^2 + W^2\right) d\varphi d\nu, \quad b_0 = 2\rho\pi \int_{-\frac{h}{2}}^{\frac{h}{2}} \int_{\varphi_t}^{\varphi_b} VW \sin\varphi d\varphi d\nu,$$

$$c_0 = \pi \int_{-\frac{h}{2}}^{\frac{h}{2}} \int_{\varphi_t}^{\varphi_b} (\eta_1 U + \eta_2 V + \eta_3 W + \eta_4)\, d\varphi d\nu, \quad c_1 = \pi \int_{-\frac{h}{2}}^{\frac{h}{2}} \int_{\varphi_t}^{\varphi_b} (\eta_5 U + \eta_6 V + \eta_7 W + \eta_8)\, d\varphi d\nu,$$

$$\begin{aligned}
\eta_1 &= \frac{GU}{(\rho_1+\nu)^2} + \frac{1}{(\rho_2+\nu)\sin\varphi}\left[\frac{2GU'\cos\varphi}{\rho_1+\nu} - \frac{4GU + W\sin\varphi\cos\varphi}{(\rho_2+\nu)\sin\varphi} + \frac{W'\sin\varphi}{\rho_1+\nu}\right] \\
&+ \frac{1}{\rho_1+\nu}\left[(2G+\lambda)\left(\frac{U'}{\rho_1+\nu} - \frac{U'\rho_1'}{(\rho_1+\nu)^2} + \frac{-U\sin\varphi + U'\cos\varphi}{(\rho_2+\nu)\sin\varphi} - \frac{U\cos\varphi\rho_2'}{(\rho_2+\nu)^2\sin\varphi}\right.\right. \\
&\left.\left. - \frac{U\cos^2\varphi}{(\rho_2+\nu)\sin^2\varphi}\right) - \frac{2GU}{\rho_1+\nu}\right] - \frac{2(2G+\lambda)\rho_1'}{\rho_1+\nu}\left[\frac{U'}{\rho_1+\nu} + \frac{U\cos\varphi}{(\rho_2+\nu)\sin\varphi}\right] \\
\eta_2 &= \left[-\frac{V}{\rho_1+\nu} - \frac{V\sin\varphi - 2W}{(\rho_2+\nu)\sin\varphi}\right]\lambda + \frac{1}{(\rho_2+\nu)\sin\varphi}\left[-\frac{2G(V\sin\varphi + 2W)}{\rho_2+\nu} + \frac{G(2\sin\varphi - 4V)}{(\rho_2+\nu)\sin\varphi}\right. \\
&\left. + \frac{GV'\cos\varphi}{\rho_1+\nu}\right] + \frac{G}{\rho_1+\nu}\left[\frac{V'-2V}{\rho_1+\nu} - \frac{V'\rho_1'}{(\rho_1+\nu)^2} + \frac{-2V\sin\varphi + 4W}{(\rho_2+\nu)\sin\varphi}\right] + \frac{GV'\rho_1'}{(\rho_1+\nu)^3} \\
\eta_3 &= -\frac{2GV - VW\sin\varphi}{(\rho_2+\nu)^2\sin\varphi} + \frac{1}{(\rho_2+\nu)\sin\varphi}\left[\frac{2G(-W\sin\varphi + 2V)}{\rho_2+\nu} + \frac{2G(2V\sin\varphi - 4W)}{(\rho_2+\nu)\sin\varphi}\right. \\
&\left. - \frac{GW\cos^2\varphi}{(\rho_2+\nu)\sin\varphi} + \frac{3W'\cos\varphi}{\rho_1+\nu} + \lambda\left(\frac{2V}{\rho_1+\nu} + \frac{2V\sin\varphi - 4W}{(\rho_2+\nu)\sin\varphi}\right)\right] + \frac{1}{\rho_1+\nu}\left[\frac{-GW\sin\varphi + 2GV}{(\rho_2+\nu)\sin\varphi}\right. \\
&\left. - \frac{G}{(\rho_2+\nu)\sin\varphi}\left(4U - \left(\frac{W\cos\varphi}{(\rho_2+\nu)\sin\varphi} - \frac{W'}{\rho_1+\nu}\right)(\rho_2'\sin\varphi + (\rho_2+\nu)\cos\varphi)\right)\right] \\
&- \frac{\rho_1'}{(\rho_1+\nu)^2}\left(\frac{W'}{\rho_1+\nu} - \frac{W\cos\varphi}{(\rho_2+\nu)\sin\varphi}\right) \\
\eta_4 &= \rho\left(U^2\cos^2\varphi + V^2\sin^2\varphi + W^2\right)\Omega^2 \\
\eta_5 &= \frac{GV'}{(\rho_1+\nu)^2} - \frac{2G}{(\rho_2+\nu)\sin\varphi}\left[\frac{V\cos\varphi - W'}{\rho_1+\nu} - \frac{U}{\rho_2+\nu} + \frac{W\cos\varphi}{(\rho_2+\nu)\sin\varphi}\right] \\
&+ \frac{1}{\rho_1+\nu}\left[(2G+\lambda)\left(-\frac{V'}{\rho_1+\nu} - \frac{V'\rho_1'}{(\rho_1+\nu)^2} + \frac{-V'\sin\varphi - V\cos\varphi + 2W'}{(\rho_2+\nu)\sin\varphi} - \frac{-V\sin\varphi + 2W\rho_2'}{(\rho_2+\nu)^2\sin\varphi}\right.\right. \\
&\left.\left. - \frac{-V\sin\varphi + 2W\cos^2\varphi}{(\rho_2+\nu)\sin^2\varphi}\right) - \frac{2GV'}{\rho_1+\nu}\right] - \frac{2(2G+\lambda)\rho_1'}{\rho_1+\nu}\left[-\frac{V}{\rho_1+\nu} + \frac{-V\sin\varphi + 2W}{(\rho_2+\nu)\sin\varphi}\right] \\
\eta_6 &= \left[-\frac{U'}{(\rho_1+\nu)^2} - \frac{U\cos\varphi}{(\rho_2+\nu)^2\sin\varphi}\right]\lambda - \frac{G}{(\rho_2+\nu)\sin\varphi}\left[\frac{2U\cos\varphi}{\rho_2+\nu} + \frac{U\cos\varphi}{\rho_1+\nu}\right] \\
&+ \frac{G}{\rho_1+\nu}\left[-\frac{3U'}{\rho_1+\nu} - \frac{U\rho_1'}{(\rho_1+\nu)^2} - \frac{2U\cos\varphi}{(\rho_2+\nu)\sin\varphi}\right] + \frac{GU\rho_1'}{(\rho_1+\nu)^3} \\
\eta_7 &= \frac{1}{(\rho_2+\nu)\sin\varphi}\left[\frac{10GU\cos\varphi}{(\rho_2+\nu)\sin\varphi} + \left(\frac{3U'}{\rho_1+\nu} + \frac{2U\cos\varphi}{(\rho_2+\nu)\sin\varphi}\right)\lambda\right] + \frac{2G}{\rho_1+\nu}\left[\frac{-W\cos\varphi}{(\rho_2+\nu)\sin\varphi} + \frac{W'}{\rho_1+\nu}\right. \\
&\left. - \frac{U\rho_2'\sin\varphi + U(\rho_2+\nu)\cos\varphi}{(\rho_2+\nu)^2\sin^2\varphi}\right] + \frac{2GU\rho_1'}{(\rho_1+\nu)(\rho_2+\nu)^2\sin\varphi} \\
\eta_8 &= -2\rho VW\sin\varphi\Omega', \quad U' = \frac{dU}{d\varphi}, \quad V' = \frac{dV}{d\varphi}, \quad W' = \frac{dW}{d\varphi}, \quad \rho_1' = \frac{d\rho_1}{d\varphi}, \quad \rho_2' = \frac{d\rho_2}{d\varphi}
\end{aligned}$$

To sum up, the zero bias stability of the prototype is 7.862°/h, and the angle random walk is about 1.487°/$h^{1/2}$. This method can guarantee the stability of gyro while satisfying a large number of processes. This result is the based on the standard of IEEE Std 1431-2004 (IEEE Standard Specification Format Guide and Test Procedure for Coriolis

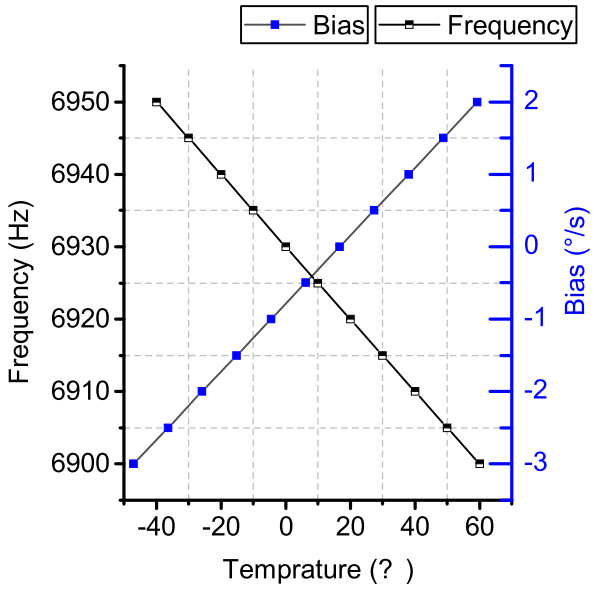

FIGURE 23. Temperature test result.

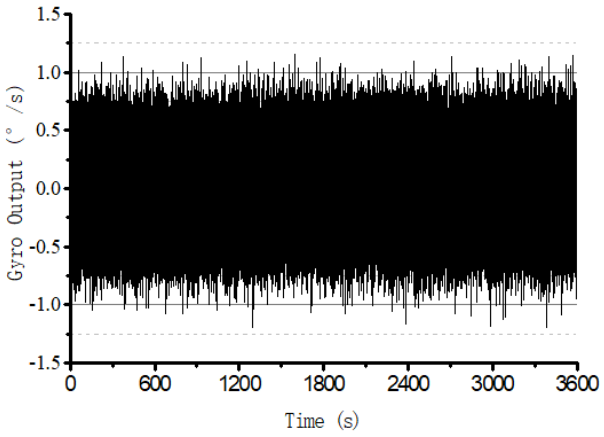

FIGURE 24. Zero bias test result.

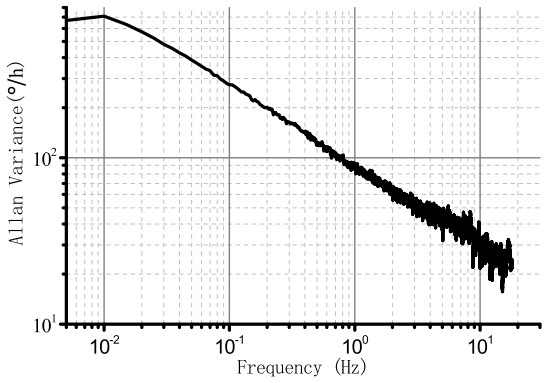

FIGURE 25. Allan variance calculation results.

Vibratory Gyros). At the last, using the same method to test this prototype on the different day. The result is:

(1) The range of gyro is 3600°/s, the scale factor linear is 1.2%, the zero bias stability of the prototype is 7.321°/h, and the angle random walk is about 1.231°/h$^{1/2}$.

(2) The range of gyro is 3600°/s, the scale factor linear is 1.0%, the zero bias stability of the prototype is 8.953°/h, and the angle random walk is about 1.329°/h$^{1/2}$.

VI. CONCLUSION

The core of the research on the metal shell resonator gyro is its theoretical modeling and analysis. b This article conducts the research on the sensitive mechanism of metal shell vibratory gyroscope, expounds the research ideas and the basic working principle of the metal shell vibratory gyroscope, and analyzes the characteristics of the gyroscope. In addition, this paper mainly solves the problem of angular rate measurement with large range and high overload; Based on the Kirchhoff-Love hypothesis, the mechanical expression of the structure of the surface of the resonator is established by means of orthogonal coordinate system, which includes stress-strain relation, strain-displacement relation and stress-displacement relation, and finally establish the equilibrium differential equation; On the basis of the equilibrium differential equation, the natural vibration characteristic of the resonator is analyzed, and the vibration mode function is deduced, and the vibration mode function is verified by simulation; And then, We carry out the modal analysis of the resonator, grasp the basic frequency of the resonator, the vibration mode and the distribution of the rigid shaft system, and determine the working mode; At the last, on the basis of modal analysis and modal analysis, the dynamic equations of the resonator are established under the action of Coriolis force. The equations are solved by the Bubnov-Galerkin method, and the resonator precession factor and natural vibration frequency are obtained. The metal shell resonator gyro is tested, and the Resonator characteristics meet the design requirements. The gyro range is 3600°/s, the zero bias stability is about 7.862°/h, and the angle random walk is about 1.487°/h$^{1/2}$.

APPENDIX

m_0, c_0, η_1, η_2, η_3, η_4, η_5, η_6, η_7, and η_8, shown at the top of the previous page.

REFERENCES

[1] N. Liu, Z. Su, and Q. Li, "Design and experiment of a novel bell-shaped vibratory gyro," *Sens. Actuators A, Phys.*, vol. 238, pp. 37–50, Feb. 2016.
[2] N. Liu, Z. Su, Q. Li, M. Fu, H. Liu, and J. Fan, "Characterization of the bell-shaped vibratory angular rate gyro," *Sensors*, vol. 13, no. 8, pp. 10123–10150, 2013.
[3] A. D. Challoner, H. H. Ge, and J. Y. Liu, "Boeing disc resonator gyroscope," in *Proc. IEEE/ION Position, Location Navigat. Symp.-PLANS*, May 2014, pp. 504–514.
[4] D. Xiao, X. Zhou, Q. Li, Z. Hou, X. Xi, Y. Wu, and X. Wu, "Design of a disk resonator gyroscope with high mechanical sensitivity by optimizing the ring thickness distribution," *J. Microelectromech. Syst.*, vol. 25, no. 4, pp. 606–616, Aug. 2016.
[5] Q. Li, D. Xiao, X. Zhou, Y. Xu, M. Zhuo, Z. Hou, K. He, Y. Zhang, and X. Wu, "0.04 degree-per-hour MEMS disk resonator gyroscope with high-quality factor (510 k) and long decaying time constant (74.9 s)," *Microsyst. Nanoeng.*, vol. 4, no. 1, 32, 2018.
[6] W. S. Watson, "Vibratory gyro skewed pick-off and driver geometry," in *Proc. IEEE/ION Position, Location Navigat. Symp. (PLANS)*, May 2010, pp. 171–179.
[7] W. S. Watson, "Vibrating inertial rate sensor utilizing skewed drive or sense elements," U.S. Patent 7 526 957 B2, May 5, 2009.

[8] A. M. Shkel, "Type I and type II micromachined vibratory gyroscopes," in *Proc. IEEE/ION Position, Location, Navigat. Symp.*, Apr. 2006, pp. 586–593.
[9] V. V. Chikovani, Y. A. Yatsenko, A. S. Barabashov, P. I. Marusyk, E. O. Umakhanov, and V. N. Taturin, "Improved accuracy metallic resonator CVG," *IEEE Aerosp. Electron. Syst. Mag.*, vol. 24, no. 5, pp. 40–43, May 2009.
[10] V. V. Chikovani, Y. A. Yatzenko, and V. A. Kovalenko, "Coriolis force gyroscope with high sensitivity," U.S. Patent 7 513 156 B2, Apr. 7, 2007.
[11] N. Liu and Z. Su, "Simulative analysis on vibrator's characteristics of cupped wave gyro," *J. Syst. Simul.*, vol. 25, no. 7, pp. 1657–1662, 2013.
[12] P. W. Loveday, "Analysis and compensation of imperfection effects in piezoelectric vibratory gyroscopes," Ph.D. dissertation, Virginia Polytech. Inst. State Univ., Blacksburg, VA, USA, 1999.
[13] D. Kristiansen, "Modeling of cylinder gyroscopes and observer design for nonlinear oscillations," Ph.D. dissertation, Dept. Eng. Cybern., Norwegian Univ. Sci. Technol., Trondheim, Norway, 2000.
[14] P. W. Loveday and C. A. Rogers, "Free vibration of elastically supported thin cylinders including gyroscopic effects," *J. Sound Vib.*, vol. 217, no. 3, pp. 547–562, 1998.
[15] X. Xi, X. Wu, Y. Zhang, X. Zhou, X. Wu, and Y. Wu"A study on Q factor of the trimmed resonator for vibratory cupped gyroscopes," *Sens. Actuators A, Phys.*, vol. 218, pp. 23–32, Oct. 2014.
[16] V. A. Matveev, M. A. Basarab, and A. V. Alekin, *Solid State Wave Gyro*. Beijing, China: National Defense Industry Press, 2009.
[17] H. Liu, Z. Su, and N. Liu, "Research on the conical resonator of a bell vibratory gyroscope under axial impact," *J. Vibroeng.*, vol. 16, no. 4, pp. 2054–2061, 2014.
[18] Ö. Civalek, "An efficient method for free vibration analysis of rotating truncated conical shells," *Int. J. Pressure Vessels Piping*, vol. 83, no. 1, pp. 1–12, 2006.
[19] L. Hua, "Frequency characteristics of a rotating truncated circular layered conical shell," *Compos. Struct.*, vol. 50, no. 1, pp. 59–68, 2000.
[20] J. H. Kang, *Three-Dimensional Vibration Analysis of Thick Shells of Revolution With Arbitrary Curvature and Variable Thickness*. Columbus, OH, USA: The Ohio State Univ., 1997.
[21] J. H. Kang and A. W. Leissa, "Three-dimensional vibration analysis of thick hyperboloidal shells of revolution," *J. Sound Vib.*, vol. 282, nos. 1–2, pp. 277–296, 2005.
[22] C. F. Sh, *Axis Shell Vibratory Gyro*. Beijing, China: National Press, 2013.
[23] H. S. Tzou and J. H. Ding, "Optimal control of precision paraboloidal shell structronic systems," *J. Sound Vib.*, vol. 276, nos. 1–2, pp. 273–291, 2004.
[24] D. Kristiansen, "Modeling of cylinder gyroscopes and observer design for nonlinear oscillations," Norwegian Univ. Sci. Technol., Trondheim, Norway, Tech. Rep., 2000.
[25] M. Shatalov and C. Coetzee, "Dynamics of rotating and vibrating thin hemispherical shell with mass and damping imperfections and parametrically driven by discrete electrodes," *Gyroscopy Navigat.*, vol. 2, no. 1, pp. 27–33, 2011.
[26] J. E. Marsden and T. J. R. Hughes, *Mathematical Foundations of Elasticity*. New York, NY, USA: Courier, 1994, pp. 90–120.
[27] W. Soedel, *Vibrations of Shells and Plates*. New York, NY, USA: CRC Press, 2004, pp. 123–160.
[28] X. Wang, H. Yue, and Z. Deng, "Active control of free paraboloidal membrane shells using photostrictive actuators," *Trans. Tianjin Univ.*, vol. 17, no. 1, pp. 6–12, 2011.
[29] D. Richards, *Advanced Mathematical Methods with Maple*. Cambridge, U.K.: Cambridge Univ. Press, 2002, pp. 56–93.
[30] M. Willatzen and L. Voon, *Separable Boundary-value Problems in Physics*. Hoboken, NJ, USA: Wiley, 2011, pp. 149–198.
[31] B. Friedland and M. Hutton, "Theory and error analysis of vibrating-member gyroscope," *IEEE Trans. Autom. Control*, vol. AC-23, no. 4, pp. 545–556, Aug. 1978.
[32] J. Ander and R. Pearson, "Application of the START vibratory gyroscope," *GEC Rev.*, vol. 1994, no. 9, pp. 168–175, 1994.
[33] W. S. Watson, "High Q angular rate sensing gyroscope," U.S. Patent 550 329 B2, Nov. 22, 2001.
[34] S. V. Joubert, M. Y. Shatalov, and T. H. Fay, "Rotating structures and Bryan's effect," *Amer. J. Phys.*, vol. 77, no. 6, pp. 520–525, 2009.
[35] Z. Lin, M. Fu, Z. Deng, N. Liu, and H. Liu, "Frequency split elimination method for a solid-state vibratory angular rate gyro with an imperfect axisymmetric-shell resonator," *Sensors*, vol. 15, no. 2, pp. 3204–3223, 2015.
[36] X. Ma and Z. Su, "Analysis and compensation of mass imperfection effects on 3-D sensitive structure of bell-shaped vibratory gyro," *Sens. Actuators A, Phys.*, vol. 224, pp. 14–23, Apr. 2015.
[37] S.-Y. Choi and J.-H. Kim, "Natural frequency split estimation for inextensional vibration of imperfect hemispherical shell," *J. Sound Vib.*, vol. 330, no. 9, pp. 2094–2106, 2011.
[38] S. McWilliam, J. Ong, and C. H. J. Fox, "On the statistics of natural frequency splitting for rings with random mass imperfections," *J. Sound Vib.*, vol. 279, nos. 1–2, pp. 453–470, 2005.
[39] F. R. Blom, S. Bouwstra, M. Elwenspoek, and J. H. J. Fluitman, "Dependence of the quality factor of micromachined silicon beam resonators on pressure and geometry," *J. Vac. Sci. Technol. B, Microelectron. Nanometer Struct. Process., Meas., Phenomena*, vol. 10, no. 1, pp. 19–26, 1992.
[40] C. Jeong, S. Seok, B. Lee, H. Kim, and K. Chun, "A study on resonant frequency and Q factor tunings for MEMS vibratory gyroscopes," *J. Micromech. Microeng.*, vol. 14, no. 11, pp. 1530–1536, 2004.
[41] I. P. Prikhodko, A. A. Trusov, and A. M. Shkel, "Compensation of drifts in high-Q MEMS gyroscopes using temperature self-sensing," *Sens. Actuators A, Phys.*, vol. 201, pp. 517–524, Oct. 2013.
[42] X. Xi, Y. Wu, Y. Zhang, X. Wu, Y. Zheng, and X. Wu, "A simple acoustic method for modal parameter measurement of the resonator for vibratory shell gyroscope," *IEEE Sensors J.*, vol. 14, no. 11, pp. 4069–4077, Nov. 2014.

NING LIU was born in 1986. He received the master's degree in automation from the Beijing Information Science and Technological University, China, in 2012. He is currently pursuing the Ph.D. degree with the School of Automation, Beijing Institute of Technology, China. His current research interests include inertial device and novel gyro sensor.

ZHONG SU received the Ph.D. degree from the Beijing Vacuum Electronics Research Institute, Beijing, China, in 1998. He is currently a Professor with Beijing Information Science and Technology University. His current research interests include control, inertial device, novel gyro sensor, and integrated navigation.